This paper must be cited as:
Carlos D. S. Brites, Bilin Zhuang, Mengistie L. Debasu, Ding Ding, Xian Qin, Fernando E. Maturi, Winnie W. Y. Lim, De Wen Soh, J. Rocha, Zhigao Yi, Xiaogang Liu*, and Luís D. Carlos, J. Phys. Chem. Lett. 2020, 11, 16, 6704–6711.
https://doi.org/10.1021/acs.jpclett.0c02147

Decoding a Percolation Phase Transition of Water at ~330 K with a Nanoparticle Ruler

Carlos D. S. Brites[1†], Bilin Zhuang[2,3†], Mengistie L. Debasu[1,4], Ding Ding[5], Xian Qin[6], Fernando E. Maturi[1], Winnie W. Y. Lim[2], De Wen Soh[2], J. Rocha[4], Zhigao Yi[6], Xiaogang Liu[6,7*] and Luís D. Carlos[1*]*

[1]Phantom-g, CICECO – Aveiro Institute of Materials, Department of Physics, Universidade de Aveiro, 3810–193 Aveiro, Portugal.

[2]Institute of High Performance Computing, Singapore 138632, Singapore.

[3]Yale-NUS College, Singapore 138527, Singapore.

[4]Department of Chemistry and CICECO – Aveiro Institute of Materials, Universidade de Aveiro, 3810–193 Aveiro, Portugal.

[5]Institute of Materials Research and Engineering, Singapore 138634, Singapore.

[6]Department of Chemistry, National University of Singapore, 117543, Singapore.

[7]Joint School of National University of Singapore and Tianjin University, International Campus of Tianjin University, Fuzhou 350207, P. R. China

†These authors contributed equally to this work.

AUTHOR INFORMATION

Corresponding Authors

* Bilin Zhuang, E-mail: zhuangbl@ihpc.a-star.edu.sg; Phone: +65 66012407

* Xiaogang Liu, E-mail: zhuangbl@ihpc.a-star.edu.sg; Phone: +351 234 360370

*Luís D. Carlos, E-mail: lcarlos@ua.pt; Phone: +351 234 370 946

ABSTRACT

Liquid water, despite its simple molecular structure, remains one of the most fascinating and complex substances. Most notably, many questions continue to exist regarding phase transitions and anomalous properties of water, which are subtle to observe experimentally. Here, we report a sharp transition in water at 330 K unveiled through experimental measurements of the instantaneous Brownian velocity of $NaYF_4$:Yb/Er upconversion nanoparticles in water. Our experimental investigations, corroborated by molecular dynamics simulations, elucidate a geometrical phase transition where a low-density-liquid (LDL) phase becomes percolated below 330 K. Around this critical temperature, we find that the sizes of the LDL clusters to be similar to the nanoparticles, confirming the role of upconversion nanoparticle as a powerful ruler for measuring the extensiveness of the LDL hydrogen-bond network and nanometer-scale spatial changes (20 to 100 nm) in liquids. Additionally, a new order parameter that unequivocally classifies water molecules into two local geometric states is introduced, providing a new tool for understanding and modelling water's many anomalous properties and phase transitions.

TOC GRAPHICS

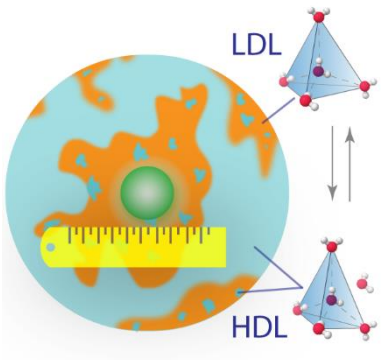

KEYWORDS Water anomaly, Nanoparticles, Luminescence nanothermometry, Brownian velocity, Molecular dynamics simulations

TEXT

Water is the most important liquid for the existence of all life on Earth. Though it is the most common liquid, it is also the most uncommon in its behaviours, exhibiting a range of anomalous properties such as increased density upon melting, density maximum at 277 K (4 ºC), reduced viscosity under pressure at below 306 K (33 ºC), high surface tension, and decreased isothermal compressibility and heat capacity with temperature at ambient conditions (minimum values at 319 K (46 ºC) and 308 K (35 ºC), respectively).[1-3] In fact, it is most questionable if life could have developed on the planet without these anomalous behaviours of water.[4-5] To explain these anomalous behaviours, the hypothesis of two organizations of hydrogen bonds competing at thermal equilibrium has been proposed.[2, 6-11] These two hydrogen-bond organizations manifest as two phases, namely the low-density liquid (LDL) and the high-density liquid (HDL), in the supercooled regime[12-15]. However, at ambient conditions, the existence of two distinct structural organizations and their implications remain elusive and controversial.

In the supercooled regime, the LDL is a predominantly low-energy hydrogen-bonded open tetrahedral configuration, while the HDL is a collection of interpenetrating shorter-ranged hydrogen-bond networks.[2, 16-19] Despite the observation of the coexistence of these two structural motifs of water through spectroscopy[20-21] and scattering measurements,[22-25] the liquid structure inferred from these experiments is strongly debated. In this context, there is an intense demand for experimental techniques to microscopically decipher water's hydrogen-bonding structure.

Recently, upconversion nanothermometry was utilized to measure the instantaneous Brownian velocity of luminescent nanocrystals suspended in liquids.[26] Since the instantaneous

Brownian velocity is sensitive to the local liquid environment, we use this method to measure the LDL motif that is known as a large tetrahedral network featuring strong cooperativity[27]. As a proof-of-concept experiment, we prepared and measured the instantaneous Brownian velocity of luminescent nanofluids containing $NaYF_4$:Yb/Er@$NaYF_4$ and $NaYF_4$:Lu/Yb/Er upconversion nanocrystals of 24 and 106 nm in diameter, respectively, dispersed in water, cyclohexene, and toluene with volume fractions (ϕ) of 0.085% and 0.066%, for the smaller and bigger nanocrystals, respectively (Figures S1,2 and Tables S1,2 in Supporting Information). The experimental set-up is similar to that in Ref. 26 and is detailed in Supporting Information. Whereas for cyclohexene and toluene the Brownian velocities increase linearly with increasing temperature, for water a bilinear behaviour with a crossover temperature T_c=329.9±0.5 K (57 ºC) for the 24 nm nanoparticles (pH=5.10±0.01) and T_c=327.4±1.2 K (54 ºC) for the 106 nm nanoparticles (pH=5.20±0.01) is clearly discerned (Figure 1a,b and Figures S9-14 in Supporting Information). Moreover, for $T>T_c$, there is a noticeable increase in the slope of the linear correlation between v and T (Table S3 in Supporting Information). These values of T_c are within the range of those reported for different physical properties of liquid water: thermal conductivity (337±5 K), proton spin-lattice relaxation time (323±5 K), refractive index (323±5 K), conductivity (326±5 K), surface tension (330±5 K), and kinetic viscosity (323±6 K),[11] as described in Figure S12 in Supporting Information. Moreover, this bilinear trend was also observed in studies involving metallic nanoparticles,[28] colloidal Ln^{3+}-based nanocrystals,[29] Eu^{3+} aqueous complexes,[30-31] and organic molecules.[32-33]

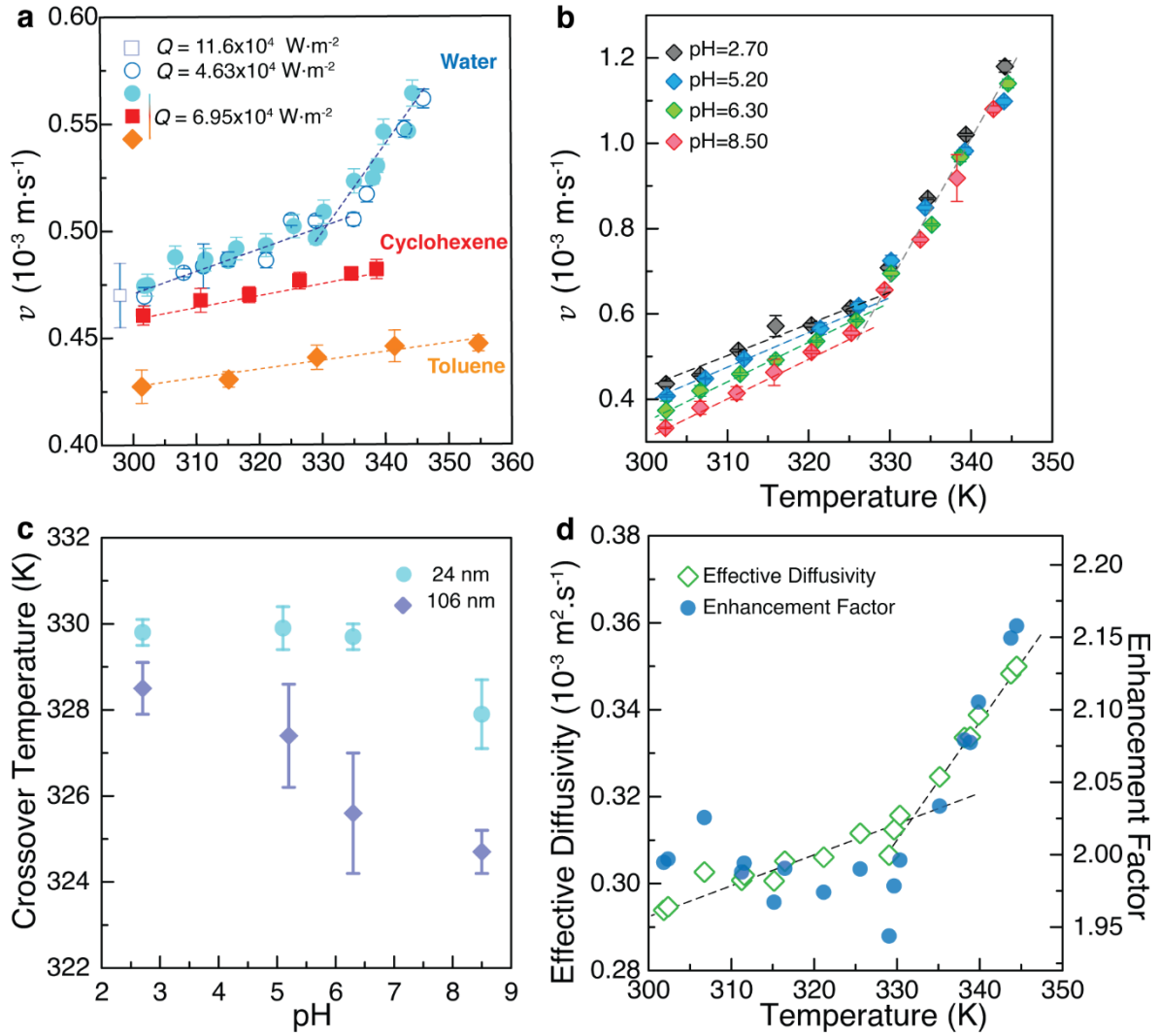

Figure 1. Dependence of the instantaneous Brownian velocity of the upconverting nanocrystals on the initial temperature and pH of the suspensions. **(a)** Temperature-dependent instantaneous Brownian velocities of the 24 nm nanoparticles suspended in water (pH=5.10±0.01), cyclohexene and toluene at initial (equilibrium) temperatures between 300 and 355 K. Vertical error bars represent mean ± SD, whereas the uncertainty in the temperature values (thermocouple accuracy, 0.1 K) is too small to be discernible in the plots. The Brownian velocities are independent of the heat flux transferred to the nanofluid (Q). The open square depicts data previously reported in similar upconverting nanoparticles[26]. The crossing of the two straight lines in the water suspensions corresponds to the crossover temperature T_c. **(b)** Temperature dependence of the Brownian velocity of the 106 nm nanoparticles in water

suspensions with distinct pH values. **(c)** The dependence on pH of the crossover temperatures. **(d)** Effective diffusivity and enhancement factor of the nanofluid with 24 nm nanoparticles (pH=5.10±0.01) with respect to pure water. All lines are the best fits to straight lines (slopes and correlation coefficients r^2 shown in Table S3 in Supporting Information).

The bilinear behaviour observed in the instantaneous velocity of nanoparticles in water indicates two regimes of nanoparticle motion, where the nanoparticles exhibit a different effective mass m^*, signaling a change in the water-nanoparticle interaction. For a nanoparticle 24 nm in diameter, m^* changes drastically at T_c, since the slope of v^2 *vs.* T for $T>T_c$ increases 4- to 5-fold relative to that for $T<T_c$ (Figure 2a and Table S4 in Supporting Information), based on the equipartition theorem $v^2 = k_B T/m^*$. Because the effective mass is influenced by both the nanoparticle's mass m_N and the mass of the fluid m_C moving cooperatively with the nanocrystal, the drastic alteration of effective mass at T_c indicates a discontinuous change in the amount of fluid that moves cooperatively with the nanoparticle. By estimating the size of the LDL motif (Section 2.1 in Supporting Information), we find a plausible mechanistic explanation that, at T_c, the sizes of LDL motifs and nanoparticles are comparable, so that below T_c the nanocrystal has to move collectively with the surrounding LDL motif (Figure 2d). In this respect, by measuring the T_c, one may use the nanoparticle as a ruler to measure the size of the LDL motif.

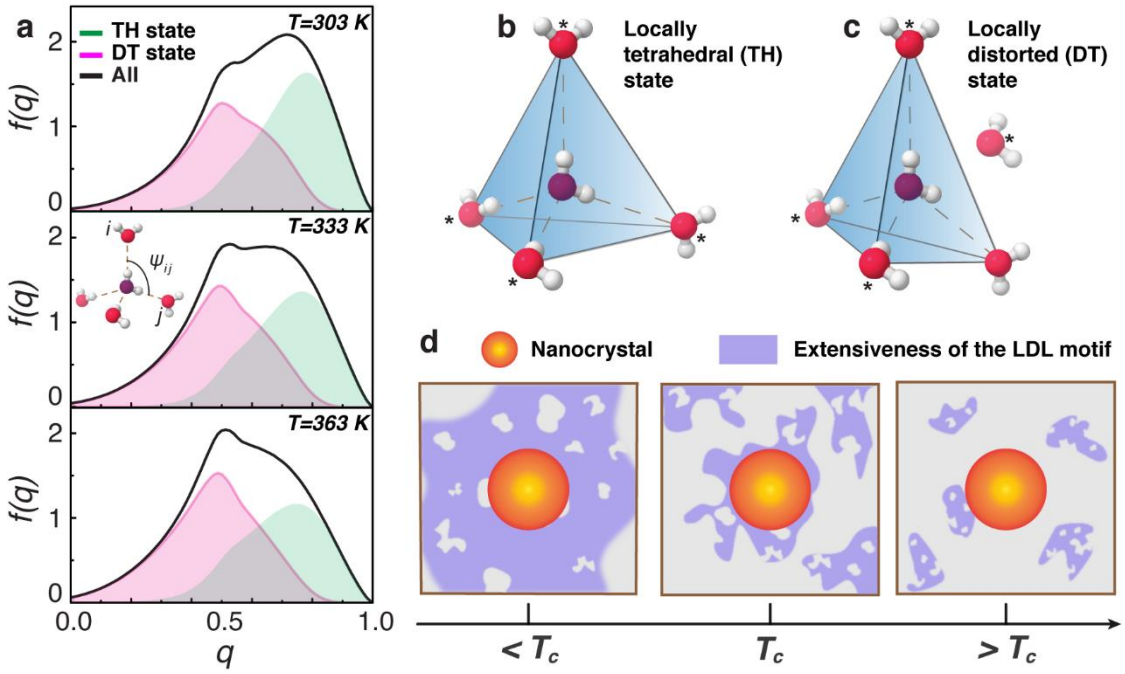

Figure 2. (**a**) The probability density function *f(q)* of the orientational order parameter *q* (Eq. 1) for water at 303 K, 333 K, and 363 K, calculated based on the molecular dynamics simulation of a cubic box of 1024 water molecules with the polarizable SWM4-NDP water model. The contributions towards *f(q)* of the locally tetrahedral (TH) state and the locally disturbed (DT) state are shown as shaded areas. (**b** and **c**) Schematics of the molecular arrangements around a water molecule (denoted with oxygen atoms in purple) in the TH-state and the DT-state. The asterisk next to the oxygen atoms denotes the four nearest neighbors. (**d**) Schematic of the length scale of the LDL motif (in purple) made up of connected TH-state molecules in comparison to the nanoparticle size (in orange).

To rationalize the transition observed in the nanoparticles' effective mass, we investigate the underlying local order of the liquid water through molecular dynamics (MD) simulation based on the polarizable SWM4-NDP water model.[34] Since tetrahedral geometry is key to distinguish the two different structures as the low-density water is thought to be more "ice-like",[35] we first examine a tetrahedral orientational order parameter *q* for each water molecule[36-37], given by:

$$q = 1 - \frac{3}{8}\sum_{j=1}^{3}\sum_{k=j+1}^{4}\left(\cos\psi_{jk} + \frac{1}{3}\right)^2 \quad (1)$$

This q-value considers the relative angular positions in the four nearest neighbors around each water molecule. The summations run over all six jk pairs among the four nearest neighbors. ψ_{jk} denotes the angle extended from the oxygen atom of the molecule to the oxygen atoms of neighbours j and k (inset of Figure 2a). The q-value grows with the tetrahedral order around a molecule, with its average value equal to one for ordinary ice and zero for an ideal gas. At ambient conditions, the probability density function *f(q)* exhibits two overlapping peaks (Figure 2a), one at higher q that decreases with temperature, and the other at lower q that increases with temperature.[37] These two peaks suggest the existence of two local structural states of water with different tetrahedral orders but, to date, their origin has not been elucidated.

Here, we introduce a new method to classify water molecules into two local structural states that give rise to the two peaks in *f(q)*. Since the peak at higher q indicates a state with a higher tetrahedral order, the positions of the four nearest neighbours are close to the vertices of a regular tetrahedron (Figure 2b). We denote this state as the locally tetrahedral (TH) state. The peak at lower q, on the other hand, indicates a state with less tetrahedral order. Owing to the open configuration in the TH-state, the second state involves an additional water molecule at an interstitial site that makes the liquid structure more tightly packed. We denote this state as the locally distorted (DT) state (Figure 2c). For a molecule in the DT-state, as the newly added molecule may become one of the four nearest neighbours, greater tetrahedral order may be found when the fifth nearest neighbour is taken into account. Therefore, we consider a generalized tetrahedral orientational order parameter q_5 to be given by the maximum value of q for any 4 out of the 5 nearest neighbours (see Supporting Information for detailed description):

$$q_5 = \max_{\substack{\text{any 4 out of} \\ \text{5 nearest} \\ \text{neighbors}}} \left[1 - \frac{3}{8} \sum_{jk} \left(cos\psi_{jk} + \frac{1}{3} \right)^2 \right] \quad (2)$$

where the summation runs over all pairs *jk* among the 4 chosen neighbours. A comparison between q and q_5 allows us to distinguish the two local structural states. In the TH state, the 4 nearest neighbours give the maximal tetrahedral order, and thus $q_5 = q$. In contrast, in the DT state, the maximal tetrahedral order arises when the 5th nearest neighbour is considered, and thus $q_5 > q$. With this rule distinguishing the two underlying states, the two closely-spaced peaks in *f(q)* (Figure 2a) are decoupled. In view of the simplicity of this classifying rule, the decoupling of the two states is considered effective, despite a slight shoulder peak that can still be discerned in the distribution of the DT state. Additional simulations based on TIP4P-FB water model[38] support the two-state behaviour observed in the SWM4-NDP model (see Supporting Information). While there have been attempts to elucidate the two-state nature of water,[7, 11, 39-41] to the best of our knowledge, this is the first rule that allows one to classify water molecules into two states without introducing *ad hoc* cut-off values or fitting parameters.

Connected TH-state molecules can form a long-ranged hydrogen-bond network, consistent with the LDL liquid structure as a large tetrahedral network featuring strong cooperativity.[27] In contrast, such cooperativity is much weaker in the HDL motif formed by the DT-state molecules, in which the hydrogen bond network is less structured and shorter-ranged. Due to the two-state nature of the hydrogen-bond network, there is necessarily a geometric percolation transition that is not thermodynamic in origin. Although the two motifs interpenetrate with each other, the network formed by TH-state molecules is long-ranged and is consequential for transport properties on a larger length scale that might be discernible. It should be noted that

the TH-state defined here is not equivalent to the low-density state that is defined elsewhere,[7, 42-43] and the connection between different two-state classifications is a subject in future work.

With nanoparticles of different sizes, the difference between T_c values of smaller and bigger nanocrystals is, in all the pH range tested, around 3 degrees (Figure 1c), suggesting a drastic change in the length scale of the LDL motif around T_c (Figure S11 in Supporting Information). This suggests that the fluctuations of LDL motifs become correlated and grow in spatial extent below T_c,[2, 44] and this could be due to the underlying percolation transition such that the LDL motif formed by TH-state molecules becomes percolated below T_c. While liquid water has been known to be a large cluster of connected hydrogen-bonded network,[45-47] here, we are concerned with the more tetrahedrally-structured network formed by TH-state molecules. Although individual hydrogen bonds in the network have short lifetime, they are likely to reform because of the favourable tetrahedral geometry. Therefore, the network formed by TH-state molecules would be more cooperative over a longer range and more persistent. Moreover, it should be noted that the LDL motifs cannot be thought as density heterogeneities measured by small-angle X-ray scattering (SAXS) measurements (dimensions of the order of 1 nm at ambient conditions).[16, 48-49] The LDL motifs are formed by a tetrahedral (ice-like) network of TH-state molecules with many empty pockets in between for the less-ordered, shorter-ranged HDL water network (dominant in ambient conditions) and, thus, are larger than the density heterogeneities measured by SAXS measurements (regions occupied by TH-state molecules exclusively). On computing the fraction of TH-state molecules (Figure 3c), x_{TH}, we notice that the fraction at T_c~330 K is close to the site percolation threshold for a diamond lattice, $x_{c,diamond}$~0.43.[50] Based on molecular configurations sampled in MD simulations, we estimate the probability of finding an LDL motif spanning the size of the 24 nm nanoparticle and observe that this probability changes rapidly from 1 to 0 around T_c (Figure 3d, calculation details in Supporting Information), consistent with the behaviour of a percolation transition.[50]

Because of this transition, there is a swift crossover in many water properties. Below T_c, LDL motifs span the liquid, increasing the structural fluctuation between the two classes of H-bond networks. Above T_c, LDL structures are short-ranged such that water behaves like a simple liquid. The crossover temperature T_c corresponds to tbe Widom line. An example of the swift crossover has been observed in the position of the second maximum of O−O pair distribution function as a function of temperature obtained through high-energy X-ray-scattering measurements[23] and our MD simulations. While the position of the first maximum r_1 increases linearly with temperature, the second maximum r_2 exhibits a bilinear behaviour with a crossover at T_c at around 330 K (Figure 3b). The agreement between X-ray diffraction and the simulation is remarkably close given that no simulation model exactly reproduces real water. The agreement between the T_c values of our experiment and of the $v^2(T)$ and $r_2(T)$ is also remarkable.

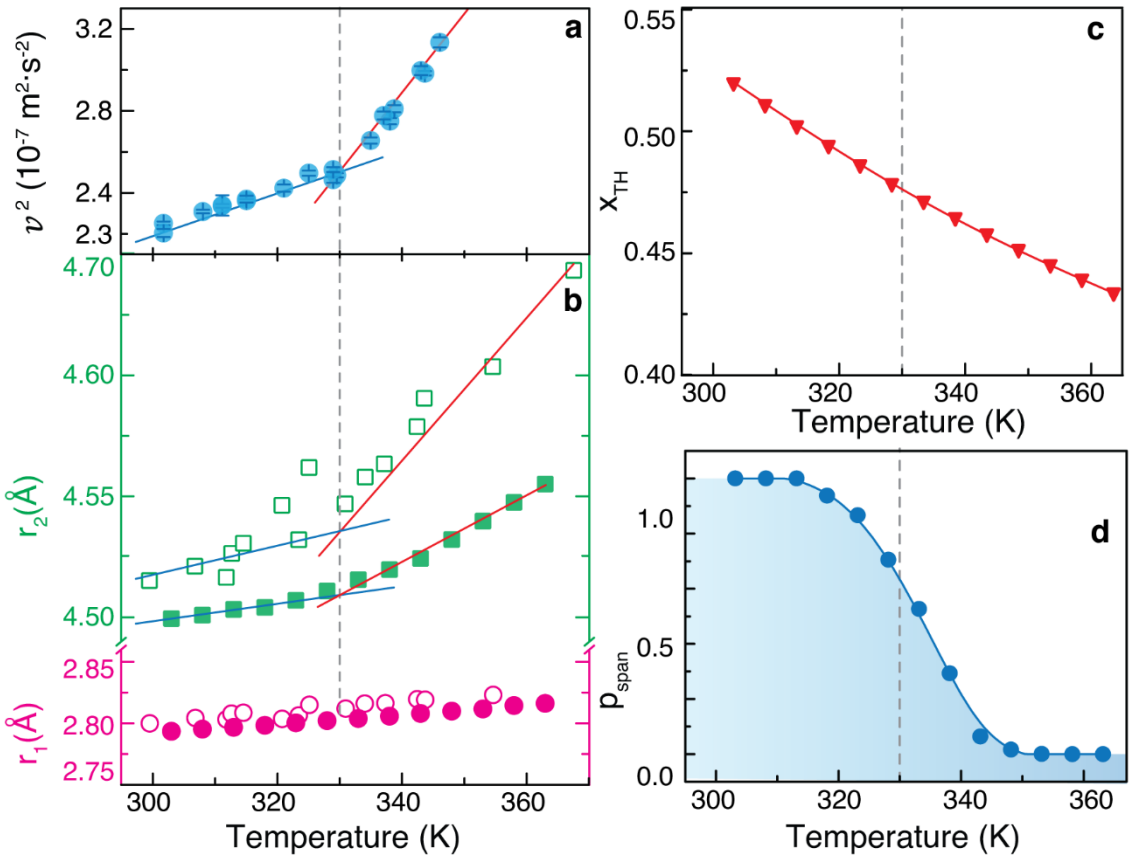

Figure 3. (**a**) Temperature dependence of the square of the instantaneous Brownian velocity of the 24 nm nanocrystals in water suspension. The straight lines are the best fit to the experimental data (r^2>0.989 and correlation coefficients in Table S7 in Supporting Information). (**b**) Simulated and experimental data on the positions of the 1st maximum (r_1) and 2nd maximum (r_2) in the O-O pair distribution function. The open circles and squares depict high-energy X-ray diffraction data adapted (without error bars) from reference[23] (points below 300 K are not displayed) and the solid circles and squares result from the MD simulations of the SWM4-NDP water model. The straight lines are the best fit to the diffraction and simulation data (correlation coefficients in Table S6 of Supporting Information). The points below 300 K (**c**) Fraction of molecules in the TH-state, x_{TH}, computed from MD simulations of SWM4-NDP water model. (**d**) Estimated probability for finding an LDL motif spanning the size of a 24 nm nanocrystal, where a strong crossover from 1 to 0 is observed at around 330 K. The dashed lines indicate the crossover temperature observed in the instantaneous Brownian velocity of 24-nm nanocrystals.

In a further set of experiments, we measured the temperature dependence of the Brownian velocity of colloidal nanocrystals in the water at pH values in the range 2.70–8.50, as illustrated in Figure 1b. Notably, for both $NaYF_4$:Yb/Er@$NaYF_4$ and $NaYF_4$:Lu/Yb/Er nanocrystals, while for $T>T_c$ the rate of increase of the Brownian velocity with temperature is independent of the nanofluid's pH, for $T<T_c$ that rate changes with the pH in such a way that the Brownian velocity increases with decreasing pH (Figure 1b). Furthermore, T_c increases with decreasing pH (Figure 1c), suggesting H_3O^+ increases the size of the LDL motif because its oxygen atoms is sp^3-hybridized and, thus, geometrically similar to TH-state water molecules. However, the observed increase of the Brownian velocity with decreasing pH for $T<T_c$ suggests that H_3O^+ destabilizes the hydrogen-bond network in the LDL motif, making the network motion less cooperative.

Using a two-plate thermal diffusion model, we can accurately describe our measured instantaneous Brownian velocity with thermal diffusion (see Supporting Information). The two-plate model predicts a linear trend of t_0 versus x_i in Figure S3 in Supporting Information and shows a linear relationship between thermal diffusivity and the predicted velocity (Figures S15-18 in Supporting Information). Extrapolating this relation using the thermal diffusivity for pure water,[51-53] we predict the thermal diffusivity for the 24 nm nanoparticles suspended in water to be enhanced more than two times, as compared to that of pure water in the same temperature range (Figure 1d). Though this large enhancement is a prediction based on thermal modelling, it is within the range of enhancements observed experimentally in some nanofluids.[54-55] It is worth noting that our numerical model highlights the fact that the temperature detected by luminescence nanocrystals obeys macroscopic thermal transport. However, to understand the exact nature of the Brownian motion at nonequilibrium conditions, comprehensive models accounting for nanoconvection and other nanoscale effects are required. Additionally, effects

of ions and the surface water structure on nanoparticles may be considered in a more comprehensive model of the system.

Using suspended nanocrystals as rulers, we have been able to detect a crossover temperature in the nanoparticle's instantaneous Brownian velocity in water, at which temperature the size of the nanoparticle and the LDL motif are comparable. This rapid change of the size of the LDL motif at around 330 K is a result of an underlying percolation transition. Since the long-range hydrogen-bond network in LDL motif is the key to decipher the behaviour of water,[56] understanding the temperature dependence of its length scale will provide insight into the properties, as well as the mechanisms, functions, and roles of water, for instance, in influencing the stability of proteins[57-58] and how they are denatured at temperatures close to the T_c value reported. Beyond the properties of water, the experimental technique of upconversion thermometry of suspended Brownian nanocrystals also has broader significance for probing interactions in fluids, for example, in the physics of the glass transition, where the cooperatively rearranging region in the glassy liquid is the central concept.[59]

EXPERIMENTAL METHODS

General description. We prepared luminescent nanofluids containing $NaYF_4$:Yb/Er@$NaYF_4$ and $NaYF_4$:Lu/Yb/Er upconversion nanocrystals of different sizes (24 and 106 nm in diameter, respectively) dispersed in water, cyclohexene, and toluene with volume fractions (ϕ) of 0.085% and 0.066%, for the smaller and bigger nanocrystals, respectively (Figures S1 and S2, Tables S1 and S2 in Supporting Information). For distinct initial equilibrium temperatures (ranging between 300 and 355 K), we heated the nanofluids and recorded their time-dependent emission spectra upon 980 nm excitation in different fixed positions along the *xx* direction (x_i=0.2–0.9 cm, i=1–6, Figures S3 and S4 in Supporting Information). For each time instance, the absolute

temperature T is calculated through the intensity ratio (the thermometric parameter Δ) between the $^2H_{11/2}\rightarrow{}^4I_{15/2}$ (I_H, 510–535 nm) and $^4S_{3/2}\rightarrow{}^4I_{15/2}$ (I_S, 535–565 nm) Er^{3+} emission bands, as[26]:

$$\frac{1}{T}=\frac{1}{T_0}-\frac{k_B}{\Delta E}\,ln\left(\frac{\Delta}{\Delta_0}\right) \qquad (3)$$

where Δ_0 is the thermometric parameter at a reference temperature T_0, k_B is the Boltzmann constant and ΔE is the energy gap between the $^2H_{11/2}$ and $^4S_{3/2}$ levels. The ΔE and Δ_0 values are determined independently by taking into account the barycenter of the $^2H_{11/2}$ (~525 nm), $^4S_{3/2}$ (~545 nm), and $^4I_{15/2}$ energy levels and from the dependence with the laser excitation power of the thermometric parameter, respectively (Figures S5 and S6 in Supporting Information). The thermometric parameter $\Delta=I_H/I_S$ increases with rising temperature[26], because the relative population of the $^2H_{11/2}$ and $^4S_{3/2}$ levels are in thermal equilibrium, following the Boltzmann's distribution[26]. In Figures S3a,b and Figure S4 in Supporting Information (where T is expressed as a reduced temperature, Supporting Information) a critical time t_{0i} is determined from the onset of change in the Er^{3+} upconversion induced by the temperature variation and the slope of the line plot between x_i and t_{0i} gives the instantaneous Brownian velocity v of the suspended upconverting nanocrystals[26] (Figure S3c,d in Supporting Information). The critical time t_{0i} is determined from the onset of the temperature variation (Figures S3 and S4 in Supporting Information) and the slope of the line plot between x_i and t_{0i} gives the instantaneous Brownian velocity v of the suspended $NaYF_4$:Yb/Er@$NaYF_4$ and $NaYF_4$:Lu/Yb/Er upconversion nanocrystals (ref[26] for details). For each fixed position x_i, we observe a marked decrease of t_{0i} with rising initial equilibrium temperature of the nanofluid (Figure S3c,d in Supporting Information for the illustrative example $x_i=0.8\times10^{-2}$ m).

Preparation of upconversion nanocrystals. $NaYF_4$:Yb/Er(18/2%)@$NaYF_4$ (average diameter 24 nm) and $NaYF_4$:Lu/Yb/Er (50/18/2%) (average diameter 106 nm) nanocrystals were synthesized by a standard co-precipitation or modified hydrothermal method according to Ref. [60]. Further experimental details are available in Supporting Information.

Operating procedure for temperature mapping. In a typical experiment, a Thorlabs quartz cuvette (CV10Q1400) was used as the container and filled with 0.50 mL of nanofluid at an initial temperature between 300 and 355 K. For water suspensions, the pH ranges from 2.70 to 8.50 (±0.01). The nanofluid's temperature is further increased through the Joule effect using a Kapton thermofoil heater (Minco) in thermal contact with one side of the cuvette. The initial temperature of the nanofluids was measured by an immersed thermocouple (I620−20147, VWR) with an accuracy of 0.1 K, accordingly to the manufacturer. Temperature increments of 10 and 15 K were generated corresponding to a heat flux transferred to the nanofluid (Q) of 4.64×10^4 and 6.96×10^4 $W\cdot m^{-2}$, respectively. A continuous-wave (CW) laser diode (980 nm, 0.5 W), positioned next to the container, is focused through an optical lens (7.5 cm focal distance) and is controlled by a moving stage with a minimum step of 0.001 mm. Under 980 nm excitation, the nanocrystals' upconversion emission is collected by a collimating lens (74-UV, Ocean Optics) and the signals are subsequently guided to the detector (Maya 2000 Pro, Ocean Optics) through a QP450-1-XSR optical fiber (Ocean Optics). The signals were denoised through the DWT procedure. Further experimental details and experimental data treatments are available in Supporting Information.

Molecular dynamics simulation of water. Molecular dynamics simulation for the polarizable SWM4-NDP water model[34] was carried out using an extended Lagrangian dynamics with a dual-Langevin thermostat[61] with OpenMM package[62]. At each temperature, the size of the cubic

simulation box was set such that the density of water molecules in the simulation box matched the density of water at atmospheric pressure (Table S6 in Supporting Information). Periodic boundary conditions are applied. For the dual-Langevin thermostat, the friction coefficients for the center-of-mass and for the internal Drude-pair degrees of freedom were 20 ps^{-1} and 1 ps^{-1}, respectively, and the temperature set for the internal Drude-pair was 1 K. The time step for the integration was 1 fs. For each randomly generated initial configuration, the system was first annealed from 373.15 K to the desired temperature in 100 equal-interval temperature steps and 1 ps per step, followed by equilibration at the desired temperature for 1 ns. Then, the configuration state of the water was sampled every 10 ps for 70 ns. The sampling was repeated independently for 8 times for each system size and temperature.

ASSOCIATED CONTENT

Supporting Information. Nanoparticle synthesis; materials characterizations; computational methods; study of the effective mass of the nanoparticles; and investigation of instantaneous Brownian velocity and thermal diffusivity.

AUTHOR INFORMATION

The authors declare no competing financial interests.

ACKNOWLEDGMENT

This work was partially developed within the scope of the project CICECO-Aveiro Institute of Materials, UIDB/50011/2020 & UIDP/50011/2020, financed by national funds through the FCT/MEC and when appropriate co-financed by FEDER under the PT2020 Partnership Agreement. Financial support from the European Union's Horizon 2020 FET Open programme under grant agreement no. 801305 and FCT (PTDC/CTM-NAN/4647/2014 and NANOHEATCONTROL - POCI-01-0145-FEDER-031469 funded by FEDER, through POCI and by national funds, OE, through FCT/MCTES) is also acknowledged. The authors acknowledge JFCBR (University of Aveiro) for his help with the signal denoising procedure. XL is grateful for the support by the Singapore Ministry of Education (MOE2017-T2-2-110), Agency for Science, Technology and Research (A*STAR) (Grant NO. A1883c0011 and A1983c0038), National Research Foundation, Prime Minister's Office, Singapore under the NRF Investigator ship programme (Award No. NRF-NRFI05-2019-0003). DD acknowledges support by A*STAR under an AME Young Individual Research Grant (Grant No.

A1884c0020). BZ acknowledges support by A*STAR under the SERC Career Development Award (Grant No. A1820g0085).

REFERENCES

1. Ball, P. Water - an enduring mystery. *Nature* **2008,** *452*, 291-292, DOI: 10.1038/452291a.
2. Nilsson, A.; Pettersson, L. G. M. The structural origin of anomalous properties of liquid water. *Nature Commun.* **2015,** *6*, 8998, DOI: 10.1038/ncomms9998.
3. Pettersson, L. G. M.; Henchman, R. H.; Nilsson, A. Water - the most anomalous liquid. *Chem. Rev.* **2016,** *116*, 7459-7462, DOI: 10.1021/acs.chemrev.6b00363.
4. Chaplin, M. Opinion - do we underestimate the importance of water in cell biology? *Nature Rev. Mol. Cell Bio.* **2006,** *7*, 861-866, DOI: 10.1038/nrm2021.
5. Pohorille, A.; Pratt, L. R. Is water the universal solvent for life? *Orig. Life Evol. Biosph.* **2012,** *42*, 405-409, DOI: 10.1007/s11084-012-9301-6.
6. Poole, P. H.; Sciortino, F.; Essmann, U.; Stanley, H. E. Phase-behavior of metastable water. *Nature* **1992,** *360*, 324-328, DOI: 10.1038/360324a0.
7. Russo, J.; Tanaka, H. Understanding water's anomalies with locally favoured structures. *Nature Commun.* **2014,** *5*, 3556, DOI: 10.1038/ncomms4556.
8. Amann-Winkel, K.; Bellissent-Funel, M. C.; Bove, L. E.; Loerting, T.; Nilsson, A.; Paciaroni, A.; Schlesinger, D.; Skinner, L. X-ray and neutron scattering of water. *Chem. Rev.* **2016,** *116*, 7570-7589, DOI: 10.1021/acs.chemrev.5b00663.
9. Gallo, P.; Arnann-Winkel, K.; Angell, C. A.; Anisimov, M. A.; Caupin, F.; Chakravarty, C.; Lascaris, E.; Loerting, T.; Panagiotopoulos, A. Z.; Russo, J.; Sellberg, J. A.; Stanley, H. E.; Tanaka, H.; Vega, C.; Xu, L. M.; Pettersson, L. G. M. Water: A tale of two liquids. *Chem. Rev.* **2016,** *116*, 7463-7500, DOI: 10.1021/acs.chemrev.5b00750.
10. Hamm, P. Markov state model of the two-state behaviour of water. *J. Chem. Phys.* **2016,** *145*, 134501, DOI: 10.1063/1.4963305.
11. Maestro, L. M.; Marques, M. I.; Camarillo, E.; Jaque, D.; Sole, J. G.; Gonzalo, J. A.; Jaque, F.; del Valle, J. C.; Mallamace, F.; Stanley, H. E. On the existence of two states in liquid water: Impact on biological and nanoscopic systems. *Int. J. Nanotechnol.* **2016,** *13*, 667-677, DOI: 10.1504/Ijnt.2016.079670.
12. Palmer, J. C.; Martelli, F.; Liu, Y.; Car, R.; Panagiotopoulos, A. Z.; Debenedetti, P. G. Metastable liquid–liquid transition in a molecular model of water. *Nature* **2014,** *510*, 385-388, DOI: 10.1038/nature13405.
13. Perakis, F.; Amann-Winkel, K.; Lehmkühler, F.; Sprung, M.; Mariedahl, D.; Sellberg, J. A.; Pathak, H.; Späh, A.; Cavalca, F.; Schlesinger, D. Diffusive dynamics during the high-to-low density transition in amorphous ice. *Proc. Natl Acad. Sci. USA* **2017,** *114*, 8193-8198, DOI: 10.1073/pnas.1705303114.
14. Lin, C.; Smith, J. S.; Sinogeikin, S. V.; Shen, G. Experimental evidence of low-density liquid water upon rapid decompression. *Proc. Natl Acad. Sci. USA* **2018,** *115*, 2010-2015, DOI: 10.1073/pnas.1716310115.
15. Woutersen, S.; Ensing, B.; Hilbers, M.; Zhao, Z.; Angell, C. A. A liquid-liquid transition in supercooled aqueous solution related to the HDA-LDA transition. *Science* **2018,** *359*, 1127-1131, DOI: 10.1126/science.aao7049.
16. Huang, C.; Wikfeldt, K. T.; Tokushima, T.; Nordlund, D.; Harada, Y.; Bergmann, U.; Niebuhr, M.; Weiss, T. M.; Horikawa, Y.; Leetmaa, M.; Ljungberg, M. P.; Takahashi, O.; Lenz, A.; Ojamae, L.; Lyubartsev, A. P.; Shin, S.; Pettersson, L. G. M.; Nilsson, A. The

inhomogeneous structure of water at ambient conditions. *Proc. Natl Acad. Sci. USA* **2009,** *106*, 15214-15218, DOI: 10.1073/pnas.0904743106.
17. Mallamace, F.; Corsaro, C.; Stanley, H. E. Possible relation of water structural relaxation to water anomalies. *Proc. Natl Acad. Sci. USA* **2013,** *110*, 4899-4904, DOI: 10.1073/pnas.1221805110.
18. Mishima, O.; Stanley, H. E. The relationship between liquid, supercooled and glassy water. *Nature* **1998,** *396*, 329-335, DOI: 10.1038/24540.
19. Soper, A. K.; Ricci, M. A. Structures of high-density and low-density water. *Phys. Rev. Lett.* **2000,** *84*, 2881-2884, DOI: 10.1103/PhysRevLett.84.2881.
20. Tokushima, T.; Harada, Y.; Takahashi, O.; Senba, Y.; Ohashi, H.; Pettersson, L. G. M.; Nilsson, A.; Shin, S. High resolution X-ray emission spectroscopy of liquid water: The observation of two structural motifs. *Chem. Phys. Lett.* **2008,** *460*, 387-400, DOI: 10.1016/j.cplett.2008.04.077.
21. Wernet, P.; Nordlund, D.; Bergmann, U.; Cavalleri, M.; Odelius, M.; Ogasawara, H.; Naslund, L. A.; Hirsch, T. K.; Ojamae, L.; Glatzel, P.; Pettersson, L. G. M.; Nilsson, A. The structure of the first coordination shell in liquid water. *Science* **2004,** *304*, 995-999, DOI: 10.1126/science.1096205.
22. Davis, J. G.; Gierszal, K. P.; Wang, P.; Ben-Amotz, D. Water structural transformation at molecular hydrophobic interfaces. *Nature* **2012,** *491*, 582-585, DOI: 10.1038/nature11570.
23. Skinner, L. B.; Benmore, C. J.; Neuefeind, J. C.; Parise, J. B. The structure of water around the compressibility minimum. *J. Chem. Phys.* **2014,** *141*, 214507, DOI: 10.1063/1.4902412.
24. Harada, Y.; Tokushima, T.; Horikawa, Y.; Takahashi, O.; Niwa, H.; Kobayashi, M.; Oshima, M.; Senba, Y.; Ohashi, H.; Wikfeldt, K. T.; Nilsson, A.; Pettersson, L. G. M.; Shin, S. Selective probing of the oh or od stretch vibration in liquid water using resonant inelastic soft-X-ray scattering. *Phys. Rev. Lett.* **2013,** *111*, 193001, DOI: 10.1103/PhysRevLett.111.193001.
25. Sellberg, J. A.; Huang, C.; McQueen, T. A.; Loh, N. D.; Laksmono, H.; Schlesinger, D.; Sierra, R. G.; Nordlund, D.; Hampton, C. Y.; Starodub, D.; DePonte, D. P.; Beye, M.; Chen, C.; Martin, A. V.; Barty, A.; Wikfeldt, K. T.; Weiss, T. M.; Caronna, C.; Feldkamp, J.; Skinner, L. B.; Seibert, M. M.; Messerschmidt, M.; Williams, G. J.; Boutet, S.; Pettersson, L. G. M.; Bogan, M. J.; Nilsson, A. Ultrafast X-ray probing of water structure below the homogeneous ice nucleation temperature. *Nature* **2014,** *510*, 381-384, DOI: 10.1038/nature13266.
26. Brites, C. D.; Xie, X.; Debasu, M. L.; Qin, X.; Chen, R.; Huang, W.; Rocha, J.; Liu, X.; Carlos, L. D. Instantaneous ballistic velocity of suspended brownian nanocrystals measured by upconversion nanothermometry. *Nat. Nanotechnol.* **2016,** *11*, 851-856, DOI: 10.1038/nnano.2016.111.
27. Errington, J. R.; Debenedetti, P. G.; Torquato, S. Cooperative origin of low-density domains in liquid water. *Phys. Rev. Lett.* **2002,** *89*, 215503, DOI: 10.1103/PhysRevLett.89.215503.
28. del Valle, J. C.; Camarillo, E.; Maestro, L. M.; Gonzalo, J. A.; Arago, C.; Marques, M.; Jaque, D.; Lifante, G.; Sole, J. G.; Santacruz-Gomez, K.; Carrillo-Torres, R. C.; Jaque, F. Dielectric anomalous response of water at 60 degrees C. *Philos. Mag.* **2015,** *95*, 683-690, DOI: 10.1080/14786435.2014.1000419.
29. Labrador-Páez, L.; Jovanovic´, D. J.; Marqués, M. I.; Smits, K.; Dolic´, S. D.; Jaque, F.; Stanley, H. E.; Dramic´anin, M. D.; García-Solé, J.; Haro-González, P.; Jaque, D. Unveiling molecular changes in water by small luminescent nanoparticles. *Small* **2017,** *13*, 1700968, DOI: 10.1002/smll.201700968.
30. Labrador-Paez, L.; Montes, E.; Pedroni, M.; Haro-Gonzalez, P.; Bettinelli, M.; Jaque, D.; Garcia-Sole, J.; Jaque, F. Effect of H_2O and D_2O thermal anomalies on the luminescence of

eu^{3+} aqueous complexes. *J. Phys. Chem. C* **2018,** *122*, 14838-14845, DOI: 10.1021/acs.jpcc.8b03937.
31. Labrador-Paez, L.; Mingoes, C.; Jaque, F.; Haro-Gonzalez, P.; Bazin, H.; Zwier, J. M.; Jaque, D.; Hildebrandt, N. pH dependence of water anomaly temperature investigated by Eu(III) cryptate luminescence. *Anal. Bioanal. Chem.* **2020,** *412*, 73-80, DOI: 10.1007/s00216-019-02215-0.
32. Catalan, J.; Gonzalo, J. A. Liquid water changes its structure at 43 degrees C. *Chem. Phys. Lett.* **2017,** *679*, 86-89, DOI: 10.1016/j.cplett.2017.04.092.
33. Catalan, J.; del Valle, J. C. Molecule 1-methyl-5-nitroindoline probes the structural change of liquid water with temperature. *ACS Omega* **2018,** *3*, 18930-18934, DOI: 10.1021/acsomega.8b02722.
34. Lamoureux, G.; Harder, E.; Vorobyov, I. V.; Roux, B.; MacKerell Jr., A. D. A polarizable model of water for molecular dynamics simulations of biomolecules. *Chem. Phys. Lett.* **2006,** *418*, 245-249, DOI: 10.1016/j.cplett.2005.10.135.
35. Kumar, P.; Wikfeldt, K. T.; Schlesinger, D.; Pettersson, L. G. M.; Stanley, H. E. The boson peak in supercooled water. *Sci. Rep.-UK* **2013,** *3*, 1980, DOI: 10.1038/srep01980.
36. Chau, P.-L.; Hardwick, A. J. A new order parameter for tetrahedral configurations. *Mol. Phys.* **1998,** *93*, 511-518, DOI: 10.1080/002689798169195.
37. Errington, J. R.; Debenedetti, P. G. Relationship between structural order and the anomalies of liquid water. *Nature* **2001,** *409*, 318-321, DOI: 10.1038/35053024.
38. Wang, L.-P.; Martinez, T. J.; Pande, V. S. Building force fields: An automatic, systematic, and reproducible approach. *J. Phys. Chem. Lett.* **2014,** *5*, 1885-1891, DOI: 10.1021/jz500737m.
39. Holten, V.; Limmer, D. T.; Molinero, V.; Anisimov, M. A. Nature of the anomalies in the supercooled liquid state of the MW model of water. *J. Chem. Phys.* **2013,** *138*, 174501, DOI: 10.1063/1.4802992.
40. Shi, R.; Russo, J.; Tanaka, H. Common microscopic structural origin for water's thermodynamic and dynamic anomalies. *J. Chem. Phys.* **2018,** *149*, 224502, DOI: 10.1063/1.5055908.
41. Wikfeldt, K. T.; Nilsson, A.; Pettersson, L. G. M. Spatially inhomogeneous bimodal inherent structure of simulated liquid water. *Phys. Chem. Chem. Phys.* **2011,** *13*, 19918-19924, DOI: 10.1039/c1cp22076d.
42. Caupin, F.; Anisimov, M. A. Thermodynamics of supercooled and stretched water: Unifying two-structure description and liquid-vapor spinodal. *J. Chem. Phys.* **2019,** *151*, 034503, DOI: 10.1063/1.5100228.
43. Singh, R. S.; Biddle, J. W.; Debenedetti, P. G.; Anisimov, M. A. Two-state thermodynamics and the possibility of a liquid-liquid phase transition in supercooled TIP4P/2005 water. *J. Chem. Phys.* **2016,** *144*, 144504, DOI: 10.1063/1.4944986.
44. Schlesinger, D.; Wikfeldt, K. T.; Skinner, L. B.; Benmore, C. J.; Nilsson, A.; Pettersson, L. G. M. The temperature dependence of intermediate range oxygen-oxygen correlations in liquid water. *J. Chem. Phys.* **2016,** *145*, 084503, DOI: 10.1063/1.4961404.
45. Stanley, H. E.; Teixeira, J. Interpretation of the unusual behavior of H_2O and D_2O at low-temperatures - tests of a percolation model. *J. Chem. Phys.* **1980,** *73*, 3404-3422, DOI: 10.1063/1.440538.
46. Geiger, A.; Stanley, H. E. Tests of universality of percolation exponents for a 3-dimensional continuum system of interacting waterlike particles. *Phys. Rev. Lett.* **1982,** *49*, 1895-1898, DOI: 10.1103/PhysRevLett.49.1895.
47. Blumberg, R. L.; Stanley, H. E.; Geiger, A.; Mausbach, P. Connectivity of hydrogen-bonds in liquid water. *J. Chem. Phys.* **1984,** *80*, 5230-5241, DOI: 10.1063/1.446593.

48. Huang, C. C.; Weiss, T. M.; Nordlund, D.; Wikfeldt, K. T.; Pettersson, L. G. M.; Nilsson, A. Increasing correlation length in bulk supercooled H_2O, D_2O, and NaCl solution determined from small angle X-ray scattering. *J. Chem. Phys.* **2010,** *133*, 134504, DOI: 10.1063/1.3495974.
49. Spah, A.; Pathak, H.; Kim, K. H.; Perakis, F.; Mariedahl, D.; Amann-Winkel, K.; Sellberg, J. A.; Lee, J. H.; Kim, S.; Park, J.; Nam, K. H.; Katayama, T.; Nilsson, A. Apparent power-law behavior of water's isothermal compressibility and correlation length upon supercooling. *Phys. Chem. Chem. Phys.* **2019,** *21*, 26-31, DOI: 10.1039/c8cp05862h.
50. Xu, X.; Wang, J.; Lv, J.-P.; Deng, Y. Simultaneous analysis of three-dimensional percolation models. *Front. Phys.* **2014,** *9*, 113-119, DOI: 10.1007/s11467-013-0403-z.
51. Sengers, J. V.; Watson, J. T. R. Improved international formulations for the viscosity and thermal conductivity of water substance. *J. Phys. Chem. Ref. Data* **1986,** *15*, 1291-1314, DOI: 10.1063/1.555763.
52. *Recommended reference materials for the realization of physicochemical properties*. Blackwell Scientific Publications: Oxford, U.K., 1987.
53. Ramires, M. L. V.; Castro, C. A. N. d.; Nagasaka, Y.; Nagashima, A.; Assael, M. J.; Wakeham, W. A. Standard reference data for the thermal conductivity of water. *J. Phys. Chem. Ref. Data* **1995,** *24*, 1377-1381, DOI: 10.1063/1.555963.
54. Pil Jang, S.; Choi, S. U. S. Effects of various parameters on nanofluid thermal conductivity. *J. Heat Transfer.* **2006,** *129*, 617-623, DOI: 10.1115/1.2712475.
55. Choi, S. U. S.; Zhang, Z. G.; Yu, W.; Lockwood, F. E.; Grulke, E. A. Anomalous thermal conductivity enhancement in nanotube suspensions. *Appl. Phys. Lett.* **2001,** *79*, 2252-2254, DOI: 10.1063/1.1408272.
56. Ben Ishai, P.; Tripathi, S. R.; Kawase, K.; Puzenko, A.; Feldman, Y. What is the primary mover of water dynamics? *Phys. Chem. Chem. Phys.* **2015,** *17*, 15428-15434, DOI: 10.1039/c5cp01871d.
57. Oleinikova, A.; Brovchenko, I. What determines the thermal stability of the hydrogen-bonded water network enveloping peptides? *J. Phys. Chem. Lett.* **2011,** *2*, 765-769, DOI: 10.1021/jz200181w.
58. Sagar, D. M.; Aoudjane, S.; Gaudet, M.; Aeppli, G.; Dalby, P. A. Optically induced thermal gradients for protein characterization in nanolitre-scale samples in microfluidic devices. *Sci. Rep.-UK* **2013,** *3*, 2130, DOI: 10.1038/srep02130.
59. Adam, G.; Gibbs, J. H. On temperature dependence of cooperative relaxation properties in glass-forming liquids. *J. Chem. Phys.* **1965,** *43*, 139-146, DOI: 10.1063/1.1696442.
60. Wang, F.; Han, Y.; Lim, C. S.; Lu, Y. H.; Wang, J.; Xu, J.; Chen, H. Y.; Zhang, C.; Hong, M. H.; Liu, X. G. Simultaneous phase and size control of upconversion nanocrystals through lanthanide doping. *Nature* **2010,** *463*, 1061-1065, DOI: 10.1038/Nature08777.
61. Jiang, W.; Hardy, D. J.; Phillips, J. C.; MacKerell, A. D.; Schulten, K.; Roux, B. High-performance scalable molecular dynamics simulations of a polarizable force field based on classical Drude oscillators in NAMD. *J. Phys. Chem. Lett.* **2011,** *2*, 87-92, DOI: 10.1021/jz101461d.
62. Eastman, P.; Friedrichs, M. S.; Chodera, J. D.; Radmer, R. J.; Bruns, C. M.; Ku, J. P.; Beauchamp, K. A.; Lane, T. J.; Wang, L.-P.; Shukla, D.; Tye, T.; Houston, M.; Stich, T.; Klein, C.; Shirts, M. R.; Pande, V. S. Open MM 4: A reusable, extensible, hardware independent library for high performance molecular simulation. *J. Chem. Theory Comput.* **2013,** *9*, 461-469, DOI: 10.1021/ct300857j.